PNAS
www.pnas.org

Supplementary Information for

Optimal transport and control of active drops

Suraj Shankar, Vidya Raju, and L. Mahadevan

Correspondence and requests for materials should be addressed to L. Mahadevan.
E-mail: lmahadev@g.harvard.edu

This PDF file includes:

Supplementary text
Figs. S1 to S3
Legends for Movies S1 to S3
SI References

Other supplementary materials for this manuscript include the following:

Movies S1 to S3

Supporting Information Text

1. Controllability and finite dimensional optimal control

We briefly outline the relevant control theoretic notions that allow us to formulate and solve the ODE formulation of the optimal transport problem. Consider a general dynamical system evolving on a smooth n-dimensional manifold $\mathcal{M}$ (the state space), of the form

$$\dot{y}(t) = f_0(y(t)) + \sum_{i=1}^{m} u_i(t) f_i(y(t)) \ , \qquad \text{[S1]}$$

where $u_i(t)$, $i = 1, \cdots, m$ are the control variables, $f_0(y)$ is a drift vector field, and $V(y) = \{f_i(y) \in T_y\mathcal{M},\ i = 1, \cdots, m\}$ is the set of nonlinear control vector fields in the tangent space ($T_y\mathcal{M}$) at a point $y \in \mathcal{M}$. This system is said to be *drift-free* if $f_0(y) = 0$, and *underactuated* if there are fewer controls than the dimensionality of the manifold, i.e., $m < \dim(\mathcal{M}) = n$. When $m < n$, let $\mathcal{V} = \cup_{y\in\mathcal{M}} \mathrm{span}\,(V(y)) \subset T\mathcal{M}$ be the m-dimensional restricted sub-bundle within the tangent bundle $T\mathcal{M} = \cup_{y\in\mathcal{M}} T_y\mathcal{M}$. In the following, we limit our attention to drift-free systems and state sufficient conditions for the existence of controls in this setting.

Definition 1.1 (Controllability) *Consider the drift-free dynamics*

$$\dot{y}(t) = \sum_{i=1}^{m} u_i(t) f_i(y(t)) \qquad \text{[S2]}$$

evolving on a smooth n-dimensional manifold $\mathcal{M}$. This system is said to be controllable if there exist controls u_i that steer the state from any initial configuration $y_0 \in \mathcal{M}$ to any final configuration $y_1 \in \mathcal{M}$.

The definition of controllability stated here does not specify the duration required to achieve the state transfer. For the special case of linear dynamical systems taking the form $\dot{y} = Ay + Bu$, controllability implies finite time controllability. In fact for this dynamics, if a prescribed state transfer is possible, it is possible in arbitrarily small time (1). However, more general systems such as S2 may be controllable, and yet not finite-time controllable.

For nonlinear dynamical systems such as in Eq. S2, the non-commutativity of the control vector fields (measured by the Lie bracket) plays a crucial role in determining the controllability of Eq. S1.

Definition 1.2 (Lie Bracket) *For two vector fields $f_i(y),\ f_j(y) \in V(y)$, their Lie bracket is defined as*

$$[f_i(y), f_j(y)] = \nabla_y f_j(y) f_i(y) - \nabla_y f_i(y) f_j(y) \ . \qquad \text{[S3]}$$

The Lie bracket dictates the tangent direction along which the dynamical system is steered under an infinitesimal cyclic actuation of the respective modulating controls u_i and u_j. The Lie *algebra* generated by the vector fields in $V(y)$, denoted by $\{f_i(y),\ 1 \le i \le m\}_{L.A}$, is constructed by equipping the vector space $V(y)$ with the Lie bracket operation (Eq. S3).

The theorem of Chow-Rashevsky (2) then provides the sufficient condition for the dynamics to be controllable.

Theorem 1.1 (Chow-Rashevsky theorem) *Consider the dynamical system (S2) defined on a smooth manifold $\mathcal{M}$ of dimension n. This system is controllable if for all $y \in \mathcal{M}$, there exist n linearly independent vector fields in the Lie algebra $\{f_i(y), 1 \le i \le m\}_{L.A.}$ generated by $\{f_i\}_{i=1}^m$, that span the tangent space $T_y\mathcal{M}$.*

Theorem 1.1 provides a test for the global notion of controllability that depends on a local quantity, the Lie bracket. For dynamics with drift such as in Eq. S1, the ability to steer in any direction in the neighbourhood of a point in $\mathcal{M}$ is restricted by the drift vector field. Hence, in such cases, local notions of accessibility and controllability need to be considered, but we do not discuss them here for simplicity (see Ref. (2) for a pedagogical introduction).

A. Optimal control problem formulation. Consider again a drift-free system (Eq. S2) on the smooth manifold $\mathcal{M}$ ($\dim(\mathcal{M}) = n$):

$$\dot{y}(t) = \sum_{i=1}^{m} u_i(t) f_i(y(t)) \equiv \mathbf{\Omega}(y(t))\mathbf{u}(t) \ , \qquad \text{[S4]}$$

where $\mathbf{\Omega}(y) = [f_1(y)\ \cdots\ f_m(y)]$, and $\mathbf{u}(t) = [u_1(t)\ \cdots\ u_m(t)]^T$. Suppose that our goal is to steer the state from $y(0)$ to $y(T)$ in finite time T, along a trajectory governed by Eq. S2, while minimizing the cost functional $\mathcal{C}$

$$\mathcal{C} = \int_0^T \mathrm{d}t\ \mathcal{L}(t, y, \mathbf{u}) \ . \qquad \text{[S5]}$$

In general, the Lagrangian $\mathcal{L}$ can depend on the state (y), the controls ($\mathbf{u}$), but also on time (t). In the simplest setting, the Lagrangian involves a quadratic form $\mathcal{L} = \mathbf{u}^T\mathbf{M}(y)\mathbf{u}$ with a state dependent positive semi-definite matrix $\mathbf{M}(y)$. Furthermore, if the controls entering $\mathcal{L}$ can be related to and eliminated in favour of the state dynamics (using Eq. S4), then the cost function takes the form

$$\mathcal{C} = \int_0^T \mathrm{d}t\ \dot{y}(t)^T g(y(t))\dot{y}(t) \ , \qquad \text{[S6]}$$

where $g(y)$ is a symmetric matrix, which when nondegenerate and positive definite, endows the manifold $\mathcal{M}$ with a metric tensor. In the case when $m = n$ and $\mathbf{\Omega}(y)$ has full rank (so is invertible), $g(y) = [\mathbf{\Omega}(y)^{-1}]^T \mathbf{M}(y)\mathbf{\Omega}(y)$ is an $n \times n$ symmetric matrix that provides a Riemannian metric (when nondegenerate) on $\mathcal{M}$. For $m < n$, the dynamics in Eq. S4 may still admit a rewriting of the cost as Eq. S6, with $g(y)$ now being an $m \times m$ symmetric positive definite matrix that defines a *sub-Riemannian* metric on the distribution $\mathcal{V} \subset T\mathcal{M}$ instead (3, 4). In either case, the problem of finding optimal solutions for the steering the state then reduces to a geometric problem, one of finding a minimizing geodesic connecting the desired initial and final states, with the appropriate metric $g(y)$ induced by the Lagrangian.

If Eq. S4 is controllable, then there exists a solution to the state transfer problem. With this assumption, we can use variational calculus to write down the first order necessary conditions for optimality of the controls, which we discuss below.

B. Pontryagin Maximum Principle. For a controllable dynamical system of the form in Eq. S4, Pontryagin's Maximum Principle (5, 6) prescribes the first order necessary conditions for optimality.

Theorem 1.2 (Pontryagin's Maximum Principle (PMP)) *Suppose there exist optimal controls* $\mathbf{u}^*(t) = [u_1^*(t) \ \cdots \ u_m^*(t)]^T$ *that minimize the cost* $\mathcal{C}$ *in Eq. S5 along trajectories satisfying Eq. S4, and the corresponding optimal state trajectory is denoted as* $y^*(t)$*. Then, there exists a costate trajectory* $p(t)$ *such that*

$$\dot{y}^* = \partial_p H(t, y^*, p, \mathbf{u}^*) \ , \tag{S7}$$

$$\dot{p} = -\partial_{y^*} H(t, y^*, p, \mathbf{u}^*) \ , \tag{S8}$$

where the Hamiltonian,

$$H(t, y, p, \mathbf{u}^*) = \max_{\mathbf{u}} \mathcal{H}(t, y, p, \mathbf{u}) \ , \tag{S9}$$

is defined as the maximum of the pre-Hamiltonian $\mathcal{H}$ *over the controls. For the cost in Eq. S5, the pre-Hamiltonian is defined as*

$$\mathcal{H}(t, y, p, \mathbf{u}) = p^T \mathbf{\Omega}(y)\mathbf{u} - \mathcal{L}(t, y, \mathbf{u}) \ . \tag{S10}$$

If the system (Eq. S2) is controllable with $m < n$, and the quadratic cost $\mathcal{C}$ can be written in terms of a positive definite metric g (Eq. S6), then we have an optimal control problem with a sub-Riemannian metric endowed by the cost on the m-dimensional distribution $\mathcal{V}$ spanned by the set of control vector fields. This is called a sub-Riemannian optimal control problem (4).

2. Reduced order dynamics and ODE drop control

Here we provide the details of the Galerkin projection calculation to obtain the finite dimensional ODE model of drop dynamics from the continuum equations. We also derive the optimal control solution for the two parameter (X, R) description of drop transport, extend the parametrization to account for drop shape and discuss the associated optimal control problem. In addition to providing a finite dimensional representation, this formulation is also ripe for the direct application of results from optimal control theory to check feasibility as well as provide, to the extent possible, analytical expressions for the transport plan.

A. Two parameter model reduction. The continuum dynamics of the drop is given by a continuity equation for the drop height $h(x, t)$ $(\int \mathrm{d}x \ h = 1)$

$$\partial_t h + \partial_x q = 0 \ , \quad q = \frac{h^3}{3\eta}\partial_x(\zeta h + \gamma \partial_x^2 h) \ , \tag{S11}$$

driven by spatiotemporally varying activity $\zeta(x, t)$ and a constant surface tension γ. As described in the main text, in the absence of activity ($\zeta = 0$), the flux vanishes when $\partial_x^3 h = 0$, i.e., $h(x, t)$ is parabolic,

$$h(x, t) = \frac{6}{R(t)^3}\left[\frac{R(t)^2}{4} - (x - X(t))^2\right] \ , \tag{S12}$$

and is parametrized by its position ($X(t) = \int \mathrm{d}x \ xh(x, t)$) and its size $R(t) = \sqrt{20\Delta(t)}$ (which is related as to the variance $\Delta(t) = \int \mathrm{d}x \ (x - X(t))^2 h(x, t)$). In order to obtain the effective dynamics of the drop in terms of $\dot{X}$ and $\dot{R}$, we take moments of Eq. S11 to get

$$\dot{X}(t) = \int_{X(t)-R(t)/2}^{X(t)+R(t)/2} \mathrm{d}x \ q(x, t) \ , \quad \dot{\Delta}(t) = \int_{X(t)-R(t)/2}^{X(t)+R(t)/2} \mathrm{d}x \ (x - X(t))q(x, t) \ . \tag{S13}$$

The limits $X(t) \pm R(t)/2$ are simply the ends of the drop, beyond which $h = 0$. This provides a closed system of equations to describe drop dynamics on the parametrized manifold invariant to surface tension flows, upon which the controlled dynamics steered by activity occurs.

B. Two dimensional ODE optimal control. Upon evaluating Eq. S13 along with the activity parametrization (Eq. 4, main text), we obtain the drop position and size dynamics to be

$$\dot{X}(t) = \frac{18\Delta\zeta(t)}{35\eta R(t)^4} \;, \quad \dot{R}(t) = -\frac{24\zeta_0(t)}{7\eta R(t)^4} \;. \tag{S14}$$

As expected, the mean and gradient components of the active stress independently control the drop size and position respectively. This, together with non-vanishing control vector fields for finite R, trivially ensure controllability. For simplicity, we shall consider the fixed end point problem, in which case the cost $\mathcal{C} = \mathcal{W}$ is simply the net dissipation, $\mathcal{W} = \int_0^T \mathrm{d}t\, \mathcal{L}$, where the Lagrangian is $\mathcal{L} = (1/\eta R^6)[(72/35)\zeta_0^2 + (54/77)\Delta\zeta^2]$. The Lagrangian is simply quadratic in the controls $(\zeta, \Delta\zeta)$, and has a strong size dependence due to the nonlinear dependence of the dissipation and friction on the height of the drop. Upon denoting the state vector as $\Psi(t) = [X(t)\ R(t)]^T$ and the costate (Lagrange multipliers) as $p(t) = [p_X(t)\ p_R(t)]^T$ to enforce the dynamical constraints in Eq. S14, a necessary condition for optimality is given by PMP. We then maximize the control Hamiltonian

$$\mathcal{H}(\Psi, p, \zeta_0, \Delta\zeta) = p_X \frac{18\Delta\zeta}{35\eta R^4} - p_R \frac{24\zeta_0}{7\eta R^4} - \mathcal{L} \;, \tag{S15}$$

over the controls to get $\zeta_0^* = -5p_R R^2/6$ and $\Delta\zeta^* = 11 p_X R^2/30$ as the maximizers. When plugged back into Eq. S15, this gives the conserved Hamiltonian (as it doesn't depend explicitly on time)

$$H(\Psi, p) \equiv \mathcal{H}(\Psi, p, \zeta_0^*, \Delta\zeta^*) = \frac{1}{7\eta R^2}\left(10p_R^2 + \frac{33}{50}p_X^2\right) \;. \tag{S16}$$

The candidate extremals for the optimal control problem are now obtained as solutions to the following Hamiltonian dynamics

$$\dot{\Psi} = \frac{\partial H}{\partial p} \;, \quad \dot{p} = -\frac{\partial H}{\partial \Psi} \;. \tag{S17}$$

For the state variables $\Psi(t)$, this gives back Eq. S14 driven by the optimal controls $(\zeta_0^*(t), \Delta\zeta^*(t))$. Translational invariance enforces that $\partial_X \mathcal{H} = 0$, hence p_X is also conserved along the optimal trajectory.

To obtain analytical expressions for the costate and optimal activity, we reparametrize time to linearize the dynamics. We define $\tau(t)$ so that

$$\dot{\tau} = \frac{1}{\eta R^2} \;, \tag{S18}$$

with the initial condition $\tau(0) = 0$. Upon writing $\chi(\tau) = X(t)$, $\rho(\tau) = R(t)$, $P(\tau) = p_R(t)$ and $p_X = p_0$ (a constant), we obtain (primes denote $\mathrm{d}/\mathrm{d}\tau$)

$$\chi' = \frac{33}{175}p_0 \;, \quad \rho' = \frac{20}{7}P \;, \quad P' = 2\eta\rho H_0 \;, \tag{S19}$$

where H_0 (constant) is the conserved value of the Hamiltonian along the optimal solution. The position equation can be integrated trivially to give $\chi(\tau) = (33p_0/175)\tau$ and the last two equations can be combined to give a linear equation for $\rho(\tau)$,

$$\rho'' - \kappa^2\rho = 0 \implies \rho(\tau) = \frac{R_T\sinh(\kappa\tau) + R_0\sinh[\kappa(\tau(T) - \tau)]}{\sinh[\kappa\tau(T)]} \;, \tag{S20}$$

where we have used the boundary conditions on the drop size ($R(0) = R_0,\ R(T) = R_T$) and defined the (as of yet) undetermined constant

$$\kappa^2 = \frac{40\eta}{7}H_0 \;. \tag{S21}$$

By imposing the boundary condition on the drop position, we obtain

$$X_T = \frac{33}{175}p_0\tau(T) \;. \tag{S22}$$

To compute the value of κ and p_0, we evaluate the conserved Hamiltonian at $t = 0$ to get

$$H_0 = \frac{1}{7\eta R_0^2}\left[10p_R(0)^2 + \frac{33}{50}p_0^2\right] \;, \tag{S23}$$

in which we can plug in the value of $p_R(0) \equiv P(0) = (7/20)\rho'(0) = (7\kappa/20\sinh[\kappa\tau(T)])\{R_T - R_0\cosh[\kappa\tau(T)]\}$ along with the expression for p_0 (from Eq. S22) to get

$$\frac{X_T}{R_0} = \sqrt{\frac{33s^2}{500\sinh^2 s}\left[\left(\frac{R_T}{R_0}\right)\left(2\cosh s - \frac{R_T}{R_0}\right) - 1\right]} \equiv \mathcal{F}\left(s, \frac{R_T}{R_0}\right) \;, \tag{S24}$$

where $s = \kappa\tau(T) > 0$ is the unknown to be solved for. Remarkably, this equation lacks any real solution for $s > 0$ if X_T/R_0 is sufficiently large for a given ratio R_T/R_0. One can show that Eq. S24 in general has either two positive solutions, one positive solution or none. By using the locus of coinciding solutions, we can compute the envelope curve of the maximal displacement for a given size change, above which Eq. S24 has no real solutions. This determines the feasibility curve for smooth optimal

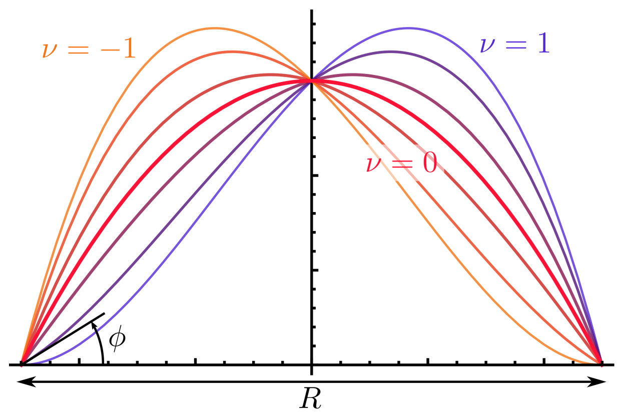

Fig. S1. The parametrization of the drop height (Eq. S27) in terms of its position (X, here centered to the origin), size (R) and an asymmetry (ν) that captures a tilt in the drop profile. For $\nu = 0$, we have a symmetric parabolic drop, and for $\nu = \pm 1$ (the extremes), we have a right or left leaning drop respectively. The asymmetry ν is related to the trailing (left most) contact angle ϕ of the drop, via $\nu = 1 - (R^2\phi/6)$.

policies (at least C^2 regularity) which is shown in Fig. 3C (main text). For large size disparities $R_T/R_0 \to \infty$, we can compute the asymptotic behaviour of this bounding curve to be a weak logarithm,

$$\left(\frac{X_T}{R_0}\right)_{\max} \simeq \sqrt{\frac{33}{500}} \ln\left(\frac{2R_T}{R_0}\right) \quad \left(\frac{R_T}{R_0} \to \infty\right) . \tag{S25}$$

By solving Eq. S24 numerically for $s = \kappa\tau(T)$, when it exists, we can use the final relation between $\tau(T)$ and T (by integrating Eq. S18) to get

$$\frac{\tau(T)}{4s\sinh^2 s}\left[(R_0^2 + R_T^2)(\sinh(2s) - 2s) + 4R_0R_T(s\cosh s - \sinh s)\right] = \frac{T}{\eta} . \tag{S26}$$

This directly gives $\tau(T)$ and hence κ (by using the now known value of s) and also H_0, thereby completing the full solution. Representative curves for the control and state dynamics are plotted in Fig. 2A-B, main text.

C. Three parameter model reduction. Here we extend our previous calculation to include a third variable that captures changes in drop shape, in addition to position and size. We parametrize the shape of the drop using a cubic polynomial that additionally captures the drop asymmetry, i.e., a tilting of the drop (see Fig. S1). Upon using $\int \mathrm{d}x\, h = 1$, we obtain

$$h(x,t) = \frac{12\nu(t)}{R(t)^4}(x - a(t))(a(t) + R(t) - x)\left[x - a(t) + \frac{R(t)(1-\nu(t))}{2\nu(t)}\right] , \tag{S27}$$

where $a(t) = X(t) - (R(t)/2) - R(t)\nu(t)/10$ is the trailing (left most) end of the drop and the dimensionless asymmetry $\nu \in [-1, 1]$ is related to the trailing (left most) contact angle $\phi(t)$ of a right moving drop via $\nu(t) = 1 - R(t)^2\phi(t)/6$ (see Fig. S1). Note that $h = 0$ at the two ends of the drop, $x = a$ and $x = a + R$, and vanishes outside this region. The drop asymmetry is restricted to the interval $\nu \in [-1, 1]$ to ensure the height in Eq. S27 is always positive. While the extreme limits of $\nu = \pm 1$ correspond to a right and left leaning drop respectively (Fig. S1), for $\nu = 0$, the drop has a symmetric parabolic profile. The position $X = \int \mathrm{d}x\, xh$ is still directly given by the mean, while the size $R(t)$ and asymmetry $\nu(t)$ of the drop can be related to the next two spatial moments of the height field $h(x,t)$ via

$$\Delta = \int \mathrm{d}x\ (x - X)^2 h = \frac{R^2}{100}[5 - \nu^2] , \tag{S28}$$

$$\Phi = \int \mathrm{d}x\ (x - X)^3 h = \frac{R^3}{3500}\nu[7\nu^2 - 15] . \tag{S29}$$

We can similarly compute spatial moments of the flux $q(x,t)$ to obtain

$$\dot{X}(t) = \int_{a(t)}^{a(t)+R(t)} \mathrm{d}x\ q(x,t) , \tag{S30}$$

$$\dot{\Delta}(t) = 2\int_{a(t)}^{a(t)+R(t)} \mathrm{d}x\ (x - X(t))q(x,t) , \tag{S31}$$

$$\dot{\Phi}(t) = 3\int_{a(t)}^{a(t)+R(t)} \mathrm{d}x\ \left[(x - X(t))^2 - \Delta(t)\right] q(x,t) . \tag{S32}$$

These equations can be inverted using Eqs. S28, S29 to obtain the complete and closed set of nonlinear dynamical equations governing the evolution of the drop position $X(t)$, size $R(t)$ and tilt $\nu(t)$. If we set $\nu = 0$ by fiat and neglect $\dot{\nu}$, then we recover

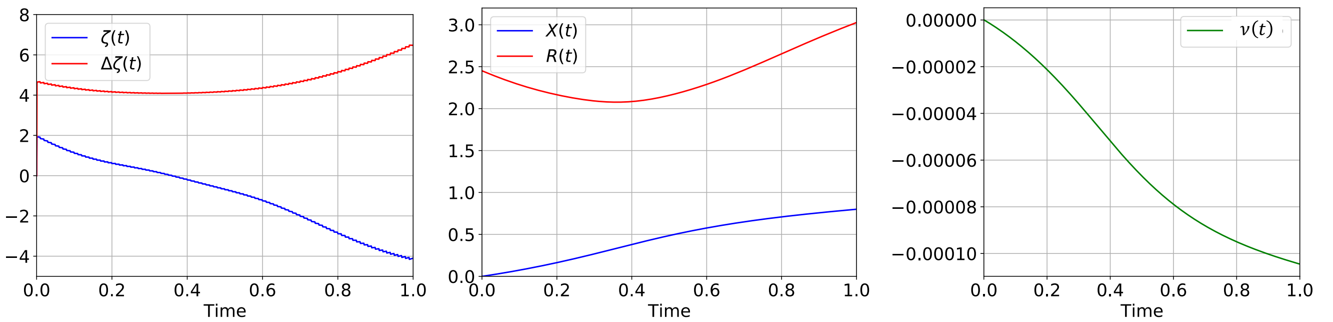

(a) Controls **(b)** Position and size **(c)** Asymmetry variable

Fig. S2. Solution to the three dimensional ODE optimal control problem with the asymmetry variable ($\nu(t)$) forced to be close to zero (when $\lambda = 10^5$) recovers the gather-move-spread strategy. The optimal control problem was solved using CasADi (7) with time step $\mathrm{d}t = 10^{-3}$. The final position was imposed as a hard terminal constraint, while the size constraint was imposed by a quadratic terminal cost with $\mu_R = 9 \times 10^{-6}$.

the coupled (X, R) dynamics given in Eq. S14. Note that, the low order Galerkin approximation employed here works best in the bulk of the drop and cannot capture boundary phenomena that occur close to the contact line. While the symmetric drop parametrized by just X, R (Eq. S12) corresponds to an effective zero mode of capillary forces (atleast within the bulk of the drop, size change is affected by γ when the contact angle and boundary effects are taken into account), in the presence of drop asymmetry ($\nu \neq 0$), this is no longer the case and surface tension forces will be present even in the bulk of the drop. In order to avoid complications from surface tension and wetting related boundary effects, we set $\gamma = 0$ for simplicity here and consider only the high active capillary number limit ($\mathrm{Ca}_\zeta \gg 1$).

D. Three dimensional ODE optimal control. The configuration space of the drop is now characterized by a three dimensional manifold $\mathcal{M}$ comprising the state variables X, R and ν. We denote the state by a column vector $\Psi(t) = [X(t)\ R(t)\ \nu(t)]^T$ evolving in $\mathcal{M} = \mathbb{R} \times \mathbb{R}^+ \times [-1, 1]$, whose dynamics constitutes a time-invariant, drift-free, and underactuated nonlinear dynamical system, given by

$$\dot{\Psi}(t) = \zeta_0(t) F(\Psi(t)) + \Delta\zeta(t) G(\Psi(t)) \ , \qquad \text{[S33]}$$

where $F(\Psi)$, $G(\Psi)$ are nonlinear control vector fields, constituting two tangent directions that are independently controlled by the mean and gradient components of the activity

$$F(\Psi) = \frac{1}{\eta R^4} \begin{bmatrix} 0 \\ F_R \\ \frac{F_\nu}{R} \end{bmatrix} = \frac{1}{\eta R^4} \begin{bmatrix} 0 \\ \frac{24[224 - (1-\nu^2)(448 - 81(1-\nu^2))]}{1001(1-\nu^2)} \\ \frac{1}{\lambda R}\frac{768\nu[28 + (1-\nu^2)(14 - 3(1-\nu^2))]}{1001(1-\nu^2)} \end{bmatrix} , \qquad \text{[S34]}$$

$$G(\Psi) = \frac{1}{\eta R^4} \begin{bmatrix} G_X \\ G_R \\ \frac{G_\nu}{R} \end{bmatrix} = \frac{1}{\eta R^4} \begin{bmatrix} \frac{18}{5005}[224 - 3(1-\nu^2)(28 - (1-\nu^2))] \\ -\frac{12\nu[352 - (1-\nu^2)(80 - (1-\nu^2))]}{1001(1-\nu^2)} \\ -\frac{1}{\lambda R}\frac{24[704 + (1-\nu^2)(32 - (1-\nu^2)(104 - 5(1-\nu^2)))]}{1001(1-\nu^2)} \end{bmatrix} . \qquad \text{[S35]}$$

Note that elements of $F(\Psi)$ and $G(\Psi)$ depend only on the size and asymmetry of the drop and are independent of its position, as expected from translational invariance. Interestingly though, F doesn't contribute to $\dot{X}$, i.e., even when the drop is spatially asymmetric ($\nu \neq 0$), a mean activity ($\zeta_0 \neq 0$) does not generate translation, although this is not prohibited by the Curie principle (8). We have introduced an additional continuation parameter λ in the dynamics of ν alone, that we tune from $\lambda = \infty$ to $\lambda = 1$ within a homotopy continuation scheme. In the $\lambda = \infty$ limit, we recover the symmetric drop system for which we have exact analytical optimal controls provided in Sec. B. Upon decreasing λ with concurrent numerical optimization using CasADi (7), we progressively deform the known symmetric drop optimal solution into the required optimal policy for the three parameter problem when $\lambda = 1$. As before, we assume the initial location of the drop is $X_0 = 0$, and initial size $R_0 = \sqrt{6}$. The final position and size are also fixed to be $X_T = 0.8$ and $R_T = 3$. While we impose a fixed end-point condition on the position ($X(T) = X_T$), we relax the terminal constraint on size with a finite cost $\mu_R = 9 \times 10^{-6}$ and leave $\nu(T)$ as a free, unconstrained variable.

We verify controllability symbolically using Mathematica (9) by checking that $\{F, G, [F, G]\}$ constitute a basis spanning the tangent space everywhere in the drop configuration space, $\mathrm{int}(\mathcal{M}) = \mathbb{R} \times (0, \infty) \times (-1, 1)$. Hence Eq. S33 is controllable and presents an underactuated sub-Riemannian optimal control problem. This implies that there exist controls $(\zeta_0, \Delta\zeta)$ that can steer any state Ψ_1 into any other state Ψ_2 in the drop configuration space.

The net dissipation is once again $\mathcal{W} = \int_0^T \mathrm{d}t\ \mathcal{L}$, with the Lagrangian

$$\mathcal{L} = \frac{1}{\eta R^6}\mathbf{u}^T\mathbf{M}\mathbf{u}\ , \tag{S36}$$

where $\mathbf{u} = [\zeta\ \Delta\zeta]^T$ and $\mathbf{M}$ is a 2×2 symmetric matrix with entries

$$M_{11}(\nu) = \frac{72}{385}\left[32 - 3(1-\nu^2)\left(8-(1-\nu^2)\right)\right]\ , \tag{S37}$$

$$M_{12}(\nu) = -\frac{72}{10010}\nu\left[160 - 3(1-\nu^2)\left(24-(1-\nu^2)\right)\right]\ , \tag{S38}$$

$$M_{22}(\nu) = \frac{18}{5005}\left[416 - (1-\nu^2)(248-27(1-\nu^2))\right]\ . \tag{S39}$$

One can easily check by explicit diagonalization that $\mathbf{M}$ is always positive definite and nondegenerate ($\det(\mathbf{M}) \neq 0$) for all $\nu \in [-1, 1]$. Compactly, the dynamics can be written as $\dot{\Psi} = \mathbf{\Omega}(\Psi)\mathbf{u}$, where

$$\begin{aligned}\mathbf{\Omega}(\Psi) &= [F\ G] \\ &= \frac{1}{\eta R^6}\begin{bmatrix} 0 & R^2 G_X \\ R^2 F_R & R^2 G_R \\ R F_\nu & R G_\nu \end{bmatrix}\ .\end{aligned} \tag{S40}$$

Further, let $V_1 = R p_R F_R + p_\nu F_\nu$ and $V_2 = R p_X G_X + R p_R G_R + p_\nu G_\nu$, and $\tilde{\mathbf{v}} = [V_1\ V_2]^T$ so that $\mathbf{w} = R\tilde{\mathbf{v}}$. The pre-Hamiltonian $\mathcal{H}(\Psi, p, \mathbf{u})$, and the optimal control $\mathbf{u}^*$ obtained by its maximization is given as

$$\mathcal{H}(\Psi, p, \mathbf{u}) = \frac{1}{\eta R^6}\left[\mathbf{w}^T\mathbf{u} - \mathbf{u}^T\mathbf{M}\mathbf{u}\right]\ , \tag{S41}$$

$$\mathbf{u}^* = \frac{1}{2}\mathbf{M}^{-1}\mathbf{w}\ , \tag{S42}$$

so that the Hamiltonian is

$$H(\Psi, p, u^*) = \frac{1}{4\eta R^6}\mathbf{w}^T\mathbf{M}^{-1}\mathbf{w}\ . \tag{S43}$$

From this, we can write the co-state equations as

$$\dot{p}_X = 0\ , \tag{S44}$$

$$\begin{aligned}\dot{p}_R &= -\frac{\partial H}{\partial R} \\ &= -\left\{-\frac{6H}{R} + \frac{1}{4\eta R^6}2\mathbf{w}^T\mathbf{M}^{-1}\frac{\partial \mathbf{w}}{\partial R}\right\} \\ &= \frac{6H}{R} - \frac{1}{2\eta R^6}\mathbf{w}^T\mathbf{M}^{-1}\left[\tilde{\mathbf{v}} + R\frac{\partial \tilde{\mathbf{v}}}{\partial R}\right]\ ,\end{aligned} \tag{S45}$$

where $\dfrac{\partial \tilde{\mathbf{v}}}{\partial R} = [p_2 F_R\ \ p_1 G_X + p_2 G_R]^T$. Moreover,

$$\begin{aligned}\dot{p}_\nu &= -\frac{\partial H}{\partial \nu} \\ &= -\frac{1}{4\eta R^6}\left\{2\mathbf{w}^T\mathbf{M}^{-1}\frac{\partial \mathbf{w}}{\partial \nu} + \mathbf{w}^T\frac{\partial \mathbf{M}^{-1}}{\partial \nu}\mathbf{w}\right\}\ .\end{aligned} \tag{S46}$$

We find the solution to the optimal transport problem by using CasADi (7). A fourth order Runge-Kutta method is used to simulate the dynamics, using time step $\mathrm{d}t = 10^{-3}$. As the optimal control solutions scale with the viscosity, we set $\eta = 0.1$ for computational convenience, without loss of generality. Since the initialization of the solver affects the optimal control solution obtained, we obtain the optimal solution presented in Fig. S3 from initial guesses for the controls: two optimal solutions for the symmetric drop and 100 randomized initial values of the control parameters at each time of discretization, uniformly sampled in the interval $[-0.5, 0.5]$. The mean stress becomes activated during earlier times causing non-monotonic changes in the drop size while the gradient component remains close to zero, where during later durations of the transport, the gradient stress drives the drop to its prescribed final location, while the shape undergoes significant change from that of a symmetric drop to a highly asymmetric one. As expected, in the limit of $\lambda \to \infty$ ($\dot{\nu}, \nu \to 0$), the protocol for the optimal transportation of the drop recovers the analytical strategy described for the symmetric drop (Fig. S2).

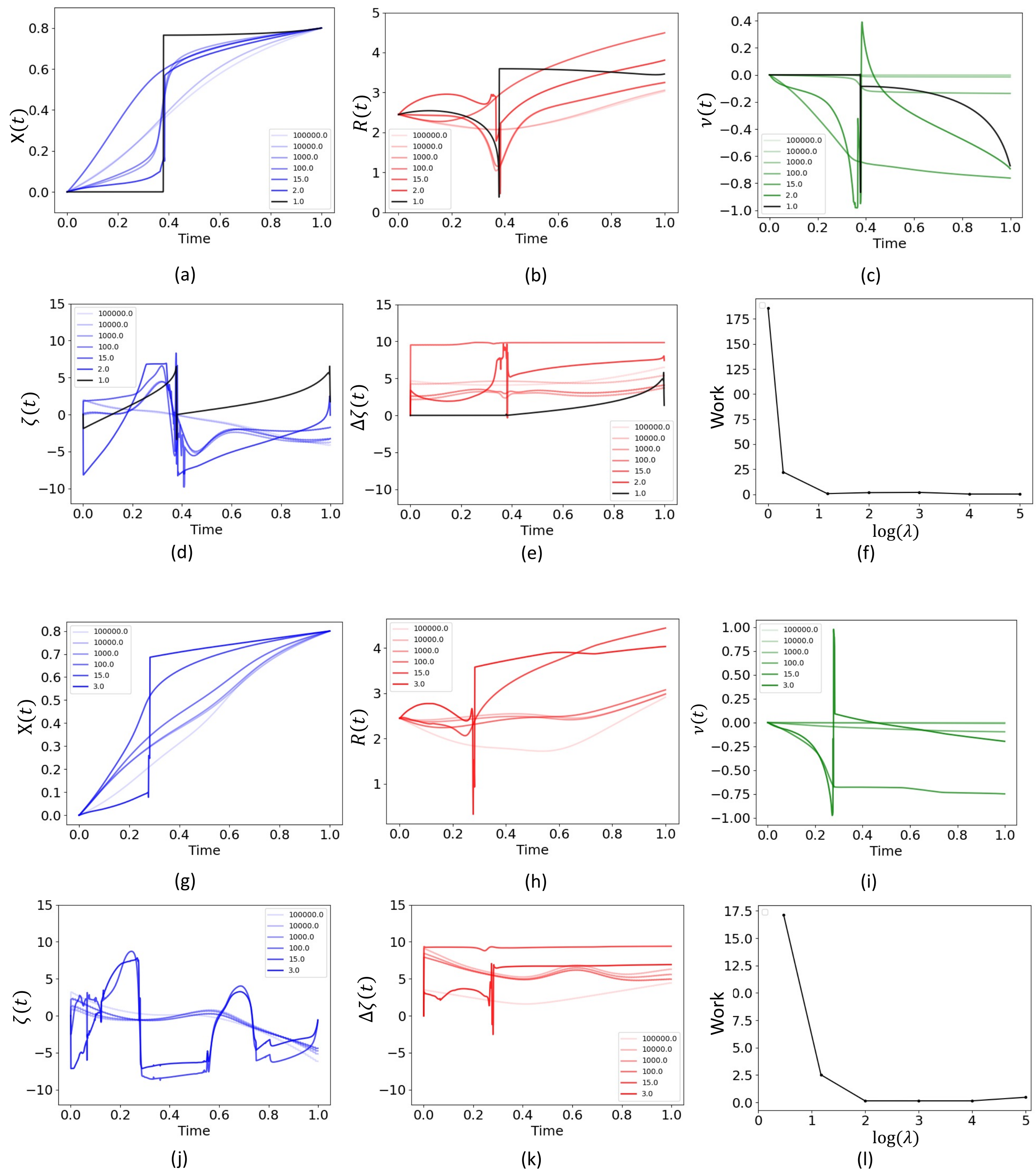

Fig. S3. Sensitivity of the optimal control solution to the parameter λ in the equation for asymmetry variable ν. The optimal solutions to the drop transport using three dimensional ODE model are obtained via sequentially optimizing while varying λ from 10^5 to 1, with the solver at the first iteration initialized by the solution to the optimal transport for the symmetric drop. The optimal control problems were solved in CasADi with time step 0.001. Plots (a)-(f) and (g)-(l) respectively show the solution to the sequential optimization problem starting with the two symmetric solutions from the two dimensional ODE optimal control problem. While the algorithm converges for initialization based on the first symmetric solution when $\lambda = 1$ corresponding to the asymmetric drop model, it does not for the second solution. We observe that in both cases for smaller values of λ, the drop undergoes rapid changes in size (R) and shape (ν), thereby affecting the numerical stability of the optimization.

3. PDE optimal control

The numerical optimization with the PDE constraint is carried out with the evolutionary algorithm CMA-ES (10), using a standard Python implementation called pycma (11). The strategy involves solving a large number of forward problems with randomly sampled controls and evolving the population to optimize a given cost, which dictates the fitness landscape. We discretize and solve the PDE as a forward problem using the finite element method in FEniCS (12, 13). We choose the domain to be an interval of length $L = 8$ with a step size $\mathrm{d}x \approx 0.01$ (resolution $N = 800$). We use a mixed semi-implicit scheme treating the nonlinear mobility explicitly using a second order Adams-Bashforth method and the linear stress tensor via Crank-Nicolson. Upon choosing $\mathrm{d}t = 5 \times 10^{-3}$ as the integration time-step and a total time $T = 1$, we use the following weak form of the PDE,

$$\left\langle \left(\frac{h_{n+1} - h_n}{\mathrm{d}t} \right), v_1 \right\rangle - \left\langle q_{n+1/2}, \partial_x v_1 \right\rangle = 0 \;, \qquad \text{[S47]}$$

where $q_{n+1/2}$ is the flux evaluated in the middle of the time step and the inner product is $\langle f, g \rangle = \int \mathrm{d}x\, fg$. We use second order Lagrange elements for our function space basis. To avoid solving a nonlinear equation, we evaluate the flux in a semi-linear fashion as

$$q_{n+1/2} = \Gamma(h_*) \left[\partial_x \sigma(h_{n+1/2}) - \Pi'(h_*) \partial_x h_{n+1/2} \right] \;, \qquad \text{[S48]}$$

where $h_* = (3h_n - h_{n-1})/2$, $h_{n+1/2} = (h_n + h_{n+1})/2$. The mobility Γ is regularized to preserve positivity of the solution (given a compliant initial condition) as (14, 15)

$$\Gamma(h) = \frac{h^4 m(h)}{h^4 + \epsilon m(h)} \;, \quad m(h) = \frac{h^3}{3\eta} \;, \qquad \text{[S49]}$$

with $\epsilon = 10^{-8}$ and viscosity $\eta = 0.1$. The stress σ includes both active and passive (capillary) contributions, with the latter providing numerical stability as well,

$$\sigma(h) = \zeta h + \gamma \mu \;, \qquad \text{[S50]}$$

$$\langle \mu, v_2 \rangle + \langle \partial_x h, \partial_x v_2 \rangle = 0 \;. \qquad \text{[S51]}$$

Both test functions, v_1 and v_2 belong to the same function space spanned by second order Lagrange elements. Hence we solve for the higher gradient term $\mu = \partial_x^2 h$ in weak form simultaneously with the continuity equation above. The constant surface tension is varied over the range $\gamma = 0.075 - 2$. We also include a disjoining pressure $\Pi(h)$ (16) to fix the contact angle for a passive, sessile drop. Along with a precursor film of thickness $\delta = 10^{-2}$, we have (17–19)

$$\Pi(h) = \frac{\mathcal{A}}{h^3} \left(1 - \frac{\delta}{h} \right) \;, \quad \Pi'(h) = \frac{\mathcal{A}}{h^5} (4\delta - 3h) \;, \qquad \text{[S52]}$$

where $\mathcal{A} = 3\gamma\delta^2 \tan^2 \phi_0$, where ϕ_0 is the required contact angle. This expression works better than $6\gamma\delta^2(1 - \cos\phi_0)$ (19) to which it is equivalent for small angles ($\phi_0 \ll 1$). We set $\phi_0 = \pi/4$ to be the equilibrium contact angle.

The boundary conditions are $\partial_x h = 0$ and $M \partial_x \sigma = 0$ at the ends of the domain (not the drop). Note, we do not track the contact line separately. Mass is naturally conserved within this formulation, which we check numerically as well. We fix $\int \mathrm{d}x\, h(x) = 1$ with the integral spanning the whole domain. The initial condition is a symmetric drop centered around the origin $X_0 = 0$ with size R_0,

$$h(x) = \begin{cases} \delta + \dfrac{6}{R_0^3}[1 - R_0\delta] \left(\dfrac{R_0^2}{4} - x^2 \right) \;, & x \in \left[-\dfrac{R_0}{2}, \dfrac{R_0}{2} \right] \\ \delta \;, \quad x \notin \left[-\dfrac{R_0}{2}, \dfrac{R_0}{2} \right] \end{cases} \;. \qquad \text{[S53]}$$

The initial size is fixed by the equilibrium contact angle to be $R_0 = \sqrt{6/\tan\phi_0} = \sqrt{6}$. We checked that this initial condition is the stable steady state of the passive dynamics if the activity is turned off.

The activity ζ is taken to be a linear profile in space

$$\zeta(x, t) = \zeta_1(t) + \zeta_2(t) x \;. \qquad \text{[S54]}$$

Note that this is in the lab frame over the entire domain and not in the drop fixed comoving frame (Eq. 4, main text). While the latter is more convenient to use for the analytical calculations, it is numerically easier to use the entirely equivalent lab fixed parametrization. The mean and gradient activity $(\zeta_0, \Delta\zeta)$ and the drop position and size (X, R) are computed using

$$\zeta_0 = \frac{1}{R} \int \mathrm{d}x\, \zeta \Theta(h - \delta_c) \;, \quad \Delta\zeta = \zeta_2 R \qquad \text{[S55]}$$

$$X = \int \mathrm{d}x\, xh \;, \quad R = \int \mathrm{d}x\, \Theta(h - \delta_c) \;, \qquad \text{[S56]}$$

where $\Theta(x)$ is the Heaviside step function, and $\delta_c = 1.1\delta = 1.1 \times 10^{-2}$ is a threshold cutoff to separate the prewetting film from the drop. We use a real element with one global degree of freedom to represent ζ_1 and ζ_2 and choose to discretize the control with a coarser time-step than required for a numerically stable integration of the PDE. This keeps the optimization manageable and avoids excessively high-dimensional searches. The control is actuated at $N_c = 100$ equi-spaced time points, and is linearly interpolated in between.

The cost function $\mathcal{C} = \mathcal{W} + \mathcal{T} + \mathcal{R}$ involves a time integrated cost from the net dissipated energy ($\mathcal{W}$), a terminal cost ($\mathcal{T}$) and a regularizing term (R), which are given by

$$\mathcal{W} = \int_0^T \mathrm{d}t \int \mathrm{d}x\, \frac{h^3}{3\eta} \left[\partial_x(\sigma - \Pi)\right]^2 \ , \tag{S57}$$

$$\mathcal{R} = \frac{\alpha}{N_c} \int_0^T \mathrm{d}t \left[(\partial_t \zeta_1)^2 + (\partial_t \zeta_2)^2\right] \ , \tag{S58}$$

$$\mathcal{T} = \mu_X \left(\frac{X(T) - X_T}{X_T}\right)^2 + \mu_R \left(\frac{R(T) - R_T}{R_T}\right)^2 \ . \tag{S59}$$

We use a trapezoidal rule to discretize the temporal integral in $\mathcal{W}$ and the spatial integral is computed using standard Gauss quadrature in FEniCS. The temporal regularization term $\mathcal{R}$ is computed easily by noting that the control is piecewise linear. Note that, $\mathcal{R} \to 0$ as $N_c \to \infty$ for fixed α and bounded time derivatives of the activity. The regularization term is used to select smoother controls and is reminiscent of minimal attention control (20). If the total cost is infinite or negative, or if $h < 0$ at any spatial point at any time, we set it to NaN, forcing CMA-ES to discard the run and reevaluate it for a random sampling of activity. We fix the following parameters,

$$X_0 = 0 \ , \quad R_0 = \sqrt{6} \ , \quad R_T = 3.0 \ , \quad \eta = 0.1 \ , \quad T = 1 \ , \quad \mu_X = \mu_R = 10^3 \ , \tag{S60}$$

and vary both the surface tension ($\gamma = 0.075 - 2$) and the terminal drop position ($X_T = 0.6,\ 0.8,\ 1.0,\ 1.2$). For the parameters chosen, both $X_T = 0.6,\ 0.8$ correspond to transport tasks for which we have a symmetric solution, while for $X_T = 1.0,\ 1.2$, the symmetric solution doesn't exist. We use multiple initializations for the optimization routine, including the two solutions (one global and one local optimum) we obtain from the symmetric problem (for the parameters where this is unavailable, we use the closest available symmetric solutions using $X_T = 0.9$, $R_T = 3$ instead), two independent sets of random activity and a sequential minimization using the best solution obtained. The random activity initializations are uniformly sampled from the interval $[-\zeta_{\max}/4, \zeta_{\max}/4]$, where $\zeta_{\max} = 20$ is the maximum permitted value of the activity to avoid numerical blow-up. We use an initial standard deviation $\Sigma_{\mathrm{dev}} = 0.2$ for both ζ_1 and ζ_2, along with a default population size of $N_{\mathrm{pop}} = 19$. The repeated function calls over the random population are parallelized over N_{pop} cores using Python's multiprocessing pool module. The maximum number of iterations is fixed at $M_{\mathrm{iter}} = 10^6$ and we set the convergence criteria to be

$$\Delta\mathcal{C} \leq \epsilon_{\mathrm{tol}} \left(\mathcal{C}^0_{\mathrm{median}} - \mathcal{C}^{\min}_{\mathrm{median}}\right) \ , \tag{S61}$$

where $\Delta\mathcal{C} = \max(\mathcal{C}) - \min(\mathcal{C})$ is the current spread in the fitness function, $\mathcal{C}^0_{\mathrm{median}}$ is the median of the initial fitness distribution and $\mathcal{C}^{\min}_{\mathrm{median}}$ is the smallest median fitness encountered throughout the optimization trajectory. We choose $\epsilon_{\mathrm{tol}} = 10^{-4}$.

4. Minimal dissipation bound

Here we derive the general bound on the minimal amount of energy that must be dissipated if a drop with bounded height achieves a nonzero displacement and size change. Consider a positive and bounded height function $h(x,t) \geq 0$ with compact nonvanishing support ($\forall t \in [0,T]$) and net unit mass ($\int \mathrm{d}x\, h = 1$) obeying the continuity equation

$$\partial_t h + \partial_x q = 0 \ , \quad q = h\langle u \rangle = \frac{h^3}{3\eta}\partial_x \sigma \ , \tag{S62}$$

driven by some arbitrary stress $\sigma = \sigma(x, t, h, \partial_x h, \cdots)$. Note, we do not specify the rheological constitutive equation for σ, nor the form of the control, so the description is entirely general to bulk stress driven drop motion*. The net dissipation in the drop is simply

$$\mathcal{W} = \int_0^T \mathrm{d}t \int \mathrm{d}x\, h\langle u \rangle \partial_x \sigma = 3\eta \int_0^T \mathrm{d}t \int \mathrm{d}x\, \frac{q^2}{h^3} \ , \tag{S63}$$

once again irrespective of the constitutive relation for σ. From Eqs. S30 and S31, we know that $\dot{X} = \int \mathrm{d}x\, q$ and $\dot{\Delta} = 2\int \mathrm{d}x\, (x - X) q$, where the position is $X = \int \mathrm{d}x\, xh$ and the variance is $\Delta = \int \mathrm{d}x\, (x-X)^2 h$. These are all finite as h is assumed to have compact support at all times. Upon integrating $\dot{X}$ and using $X(0) = X_0 = 0$ without loss of generality, we obtain,

$$|X(T)| = \left| \int_{t,x} \left(\frac{q}{h}\right) h \right| \leq \sqrt{\int_{t,x} \frac{q^2}{h^2} \int_{t,x} h^2} \ , \tag{S64}$$

where $\int_{t,x} = \int_0^T \mathrm{d}t \int \mathrm{d}x$ and we have used the Cauchy-Schwarz inequality. We can now use Hölder's inequality to write

$$\int_{t,x} h^2 \leq \|h\|_\infty \int_{t,x} h = T\|h\|_\infty \ , \tag{S65}$$

*Drop motion driven by marangoni forces or differential surface wetting are not included in this formalism as they appear as body forces and not stresses in lubrication theory.

where $\|h\|_\infty = \sup_{x,t} h(x,t)$ is the maximum height achieved by the drop at any point along its trajectory (guaranteed to be finite by mass conservation and the nonvanishing compact support). Similarly, we can use Eq. S63 and Hölder's inequality again to write

$$\int_{t,x} \frac{q^2}{h^2} \leq \|h\|_\infty \int_{t,x} \frac{q^2}{h^3} = \|h\|_\infty \frac{\mathcal{W}}{3\eta} . \quad \text{[S66]}$$

Upon combining Eqs. S64-S66 we get

$$X(T)^2 \leq \|h\|_\infty^2 \frac{T\mathcal{W}}{3\eta} . \quad \text{[S67]}$$

We can perform a similar calculation for the variance Δ. This gives (using the Cauchy-Schwarz inequality)

$$|\Delta(T) - \Delta(0)| = 2\left|\int_{t,x} q(x-X)\right| \leq 2\sqrt{\int_{t,x}\frac{q^2}{h^2}\int_{t,x} h^2(x-X)^2} . \quad \text{[S68]}$$

Hölder's inequality can now be used to simplify the right hand side,

$$\int_{t,x} h^2(x-X)^2 \leq \|h\|_\infty \int_0^T \mathrm{d}t\ \Delta(t) = \|h\|_\infty T\langle\Delta\rangle_T , \quad \text{[S69]}$$

with $\langle\Delta\rangle_T$ as the time averaged variance of the drop (also finite). This gives

$$|\Delta(T) - \Delta(0)|^2 \leq 4\frac{T\mathcal{W}}{3\eta}\|h\|_\infty^2 \langle\Delta\rangle_T . \quad \text{[S70]}$$

By combining Eqs. S67, S70, we obtain the desired lower bound on the dissipation to be

$$\mathcal{W}_{\min} \equiv \frac{3\eta}{2T\|h\|_\infty^2}\left[X(T)^2 + \frac{|\Delta(T)-\Delta(0)|^2}{4\langle\Delta\rangle_T}\right] \leq \mathcal{W} . \quad \text{[S71]}$$

5. Supplementary Movies

Movie S1. Video showing the activity controls $\{\zeta_0(t), \Delta\zeta(t)\}$, the state trajectory $\{X(t), R(t)\}$ and full drop profile $h(x,t)$ corresponding to the optimal solution computed using CMA-ES for a large active capillary number ($\mathrm{Ca}_\zeta = 383.66$), or conversely small surface tension ($\gamma = 0.15$). The optimal policy qualitatively employs a "gather-move-spread" strategy, though now with complex shape changes of the drop. The drop is initialized as a parabola centered at $X_0 = 0$, with size $R_0 = \sqrt{6}$ (equilibrium contact angle $\phi_{\mathrm{eq}} = \pi/4$) with terminal position and size fixed to $X_T = 0.8$ and $R_T = 3$ respectively. The viscosity ($\eta = 0.1$) and the total time ($T = 1$) are fixed as well.

Movie S2. Video showing the activity controls $\{\zeta_0(t), \Delta\zeta(t)\}$, the state trajectory $\{X(t), R(t)\}$ and full drop profile $h(x,t)$ corresponding to the optimal solution computed from the reduced order ODE model in Eq. 10. The activity profile plotted in Fig. 3A is used as the input for the simulation and the surface tension is set to a small value ($\gamma = 0.15$) as appropriate for the validity of the ODE model. All other parameters are kept the same ($X_0 = 0$, $R_0 = \sqrt{6}$, $X_T = 0.8$, $R_T = 3$, $\eta = 0.1$, $T = 1$) The drop trajectory is qualitatively similar to the full optimal solution (shown in Movie S1 and Fig. 4A) but not quantitatively accurate, for instance, the final drop position and size only reach about half the values set by the task.

Movie S3. Video showing the activity controls $\{\zeta_0(t), \Delta\zeta(t)\}$, the state trajectory $\{X(t), R(t)\}$ and full drop profile $h(x,t)$ corresponding to the optimal solution computed using CMA-ES for a small active capillary number ($\mathrm{Ca}_\zeta = 30.91$), or conversely small surface tension ($\gamma = 2$). The optimal policy is now quite different, with futile size oscillations that initially dissipate energy without translation and a final activity burst that advances the drop at the end of the policy. The drop is initialized as a parabola centered at $X_0 = 0$, with size $R_0 = \sqrt{6}$ (equilibrium contact angle $\phi_{\mathrm{eq}} = \pi/4$) and the terminal position and size are $X_T = 0.8$ and $R_T = 3$ respectively. The viscosity ($\eta = 0.1$) and the total time ($T = 1$) are fixed as well.

References

1. RW Brockett, *Finite dimensional linear systems.* (SIAM), (2015).
2. R Hermann, A Krener, Nonlinear controllability and observability. *IEEE Transactions on automatic control* **22**, 728–740 (1977).
3. RS Strichartz, Sub-riemannian geometry. *J. Differ. Geom.* **24**, 221–263 (1986).
4. A Agrachev, D Barilari, U Boscain, *A comprehensive introduction to sub-Riemannian geometry.* (Cambridge University Press) Vol. 181, (2019).

5. V Jurdjevic, *Geometric control theory.* (Cambridge university press), (1997).
6. L Pontryagin, *Mathematical Theory of Optimal Processes.* (CRC Press), (1987).
7. JA Andersson, J Gillis, G Horn, JB Rawlings, M Diehl, Casadi: a software framework for nonlinear optimization and optimal control. *Math. Program. Comput.* **11**, 1–36 (2019).
8. P Curie, Sur la symétrie dans les phénomènes physiques, symétrie d'un champ électrique et d'un champ magnétique. *J. de physique théorique et appliquée* **3**, 393–415 (1894).
9. WR Inc., Mathematica, Version 12.0 (2019) Champaign, IL.
10. N Hansen, *The CMA Evolution Strategy: A Comparing Review*, eds. JA Lozano, P Larrañaga, I Inza, E Bengoetxea. (Springer Berlin Heidelberg, Berlin, Heidelberg), pp. 75–102 (2006).
11. N Hansen, Y Akimoto, P Baudis, CMA-ES/pycma on Github (Zenodo, DOI:10.5281/zenodo.2559634) (2019).
12. A Logg, KA Mardal, G Wells, *Automated solution of differential equations by the finite element method: The FEniCS book.* (Springer Science & Business Media) Vol. 84, (2012).
13. M Alnæs, et al., The fenics project version 1.5. *Arch. Numer. Softw.* **3** (2015).
14. AL Bertozzi, M Pugh, The lubrication approximation for thin viscous films: the moving contact line with a'porous media'cut-off of van der waals interactions. *Nonlinearity* **7**, 1535 (1994).
15. L Zhornitskaya, AL Bertozzi, Positivity-preserving numerical schemes for lubrication-type equations. *SIAM J. on Numer. Analysis* **37**, 523–555 (1999).
16. PG De Gennes, Wetting: statics and dynamics. *Rev. modern physics* **57**, 827 (1985).
17. F Brochard-Wyart, JM Di Meglio, D Quére, PG De Gennes, Spreading of nonvolatile liquids in a continuum picture. *Langmuir* **7**, 335–338 (1991).
18. PG De Gennes, F Brochard-Wyart, D Quéré, *Capillarity and wetting phenomena: drops, bubbles, pearls, waves.* (Springer Science & Business Media), (2013).
19. AA Pahlavan, L Cueto-Felgueroso, AE Hosoi, GH McKinley, R Juanes, Thin films in partial wetting: Stability, dewetting and coarsening. *J. Fluid Mech.* **845**, 642–681 (2018).
20. RW Brockett, Minimum attention control in *Proceedings of the 36th IEEE Conference on Decision and Control.* (IEEE), Vol. 3, pp. 2628–2632 (1997).